Nanotechnology

PAPER

Berezinskii–Kosterlitz–Thouless transition in an Al superconducting nanofilm grown on GaAs by molecular beam epitaxy

IOP Publishing Nanotechnology
Nanotechnology 31 (2020) 205002 (6pp) https://doi.org/10.1088/1361-6528/ab71ba

Berezinskii–Kosterlitz–Thouless transition in an Al superconducting nanofilm grown on GaAs by molecular beam epitaxy

Guan-Ming Su[1], Bi-Yi Wu[1], Yen-Ting Fan[2], Ankit Kumar[1,3], Chau-Shing Chang[4], Ching-Chen Yeh[1], Dinesh K Patel[1], Sheng-Di Lin[2,6], Lee Chow[1,5] and Chi-Te Liang[1,4,6]

[1] Department of Physics, National Taiwan University, Taipei 106, Taiwan
[2] Department of Electronics Engineering, National Chiao Tung University, Hsinchu 300, Taiwan
[3] Department of Physics, BITS-Pilani, K. K. Birla Goa Campus, Zuarinagar, Goa 403726, India
[4] Graduate Institute of Applied Physics, National Taiwan University, Taipei 106, Taiwan
[5] Department of Physics, University of Central Florida, Orlando, FL 32816, United States of America

E-mail: sdlin@mail.nctu.edu.tw and ctliang@phys.ntu.edu.tw

Received 11 December 2019, revised 30 December 2019
Accepted for publication 30 January 2020
Published 2 March 2020

Abstract

We have performed extensive transport experiments on a 4 nm thick aluminum (Al) superconducting film grown on a GaAs substrate by molecular beam epitaxy (MBE). Nonlinear current–voltage (I–V) measurements on such a MBE-grown superconducting nanofilm show that $V \sim I^3$, which is evidence for the Berezinskii–Kosterlitz–Thouless (BKT) transition, *both* in the low-voltage ($T_{BKT} \approx 1.97$ K) and high-voltage regions ($T_{BKT} \approx 2.17$ K). In order to further study the two regions where the I–V curves are BKT-like, our experimental data are fitted to the temperature-induced vortices/antivortices unbinding model as well as the dynamical scaling theory. It is found that the transition temperature obtained in the high-voltage region is the correct T_{BKT} as confirmed by fitting the data to the aforementioned models. Our experimental results unequivocally show that I–V measurements alone may not allow one to determine T_{BKT} for superconducting transition. Therefore, one should try to fit one's results to the temperature-induced vortices/antivortices unbinding model and the dynamical scaling theory to accurately determine T_{BKT} in a two-dimensional superconductor.

Keywords: nanofilm, superconductivity, aluminum, two-dimensional, GaAs substrate

(Some figures may appear in colour only in the online journal)

1. Introduction

Superconductivity in two dimensions itself is an interesting and fundamental issue. One of the most probable reasons for this is that according to Mermin–Wagner theorem, continuous symmetries cannot be spontaneously broken at a finite temperature in systems with sufficiently short-range interactions in dimensions $d \leqslant 2$ [1]. In other words, Mermin–Wagner theorem seems to prohibit the superconducting phase transition that accompanies a symmetry breaking and a long-range correlation of the order parameter in two dimensions [1]. Nevertheless, the Berezinskii–Kosterlitz–Thouless (BKT) transition [2, 3] can occur in a two-dimensional (2D) system and allows the establishment of quasi-long-range correlation of the order parameter. The BKT physics of superconductivity is probably best characterized by nonlinear I–V dependences where I and V are the current flowing between the source and drain contacts and the voltage drops between two voltage probes, respectively. A small but finite resistance is found at temperatures below the transition temperature T_{BKT} [4, 5]. The reason for this is that in the BKT scenario, zero resistance is possible only in the zero current

[6] Authors to whom any correspondence should be addressed.

limit. Any small non-zero current exerts a force of opposite signs on vortices of opposite polarity, thereby breaking apart the most loosely bound vortex/antivortex pairs and resulting in a finite resistance (and voltage). In the region where the BKT physics manifests itself as the voltage V varies with $I^{\alpha(T)}$. The exponent $\alpha(T)$ is greater than 3 below $T_{\rm BKT}$ and is equal to 3 at $T_{\rm BKT}$ [4, 5]. Therefore, it is useful to measure the nonlinear I–V curves of a superconducting film and find the relation $V \sim I^{\alpha(T)}$ at various temperatures. When $\alpha(T) = 3$, one can experimentally determine $T_{\rm BKT.}$ The BKT transition of superconductivity has been observed in various nanofilms such as Pb atomic films [5], monolayer $NbSe_2$ [6], Ga thin films [7], and one-atom-layer Tl–Pb compound on Si(111) [8].

Aluminum (Al) is a sustainable material since it is the most abundant metal on the Earth's crust. Al ultrathin film has already found a wide variety applications in surface-enhanced Raman scattering (SERS) [9], photocatalysis [10, 11], metal-enhanced fluorescence [12], plasmonic devices [13, 14], the electrode for quantum dot light emitting diodes [15], nano-cavity [16], UV–vis chiroptical activity [17], and super-capacitors [18]. Recent advances in sample preparation have made it possible to grow high-quality Al film by molecular beam epitaxy (MBE) [13, 14, 19, 20]. In particular, an epitaxial Al film of atomic thickness can be grown on a GaAs substrate by MBE [19, 20]. Such an Al nanofilm is ideal for probing 2D physics and topological, superconducting transition in two dimensions [2–8]. Here we report extensive transport measurements on a 4 nm thick Al film grown on a GaAs substrate by MBE. Interestingly, in the nonlinear current–voltage (I–V) measurements, we have observed $V \sim I^3$, evidence for the BKT transition *both* in the low-voltage ($T_{\rm BKT} \approx 1.97$ K) and high-voltage regions ($T_{\rm BKT} \approx 2.17$ K). In order to further probe the two regions where the I–V characteristics show BKT-like behavior, we fit our experimental data to the temperature-induced vortices/antivortices model as well as the dynamical scaling theory. It is found that $T_{\rm BKT} \approx 2.17$ K determined from the data in the high voltage regime is actually the correct transition temperature since it is consistent with those measured by the aforementioned models. Thus our experimental data strongly suggest that one should fit one's experimental results to both the vortices/antivortices unbinding model and dynamical scaling model since the nonlinear I–V data ($V \sim I^3$) alone may not allow one to unequivocally determine the topological transition temperature $T_{\rm BKT}$.

2. Experimental

2.1. Al nanofilm grown by MBE

The semi-insulating GaAs substrate was first baked in our Varian Gen II MBE chamber at 200 °C for 8 h. The purpose of this process is to remove the moisture on the surface of the GaAs substrate. After that, the GaAs substrate was heated to 400 °C for 5 h to remove organic residue in a preparation chamber. The wafer was put back in the main chamber. After removing the native oxide on the GaAs substrate at 600 °C for 20 min, at 580 °C we grew a 200 nm thick undoped GaAs buffer layer. The Ga shutter was turned off. Subsequently, the GaAs surface temperature was increased to 600 °C with no As flux (As shutter was off) for 3 min in order to transform the GaAs surface into a Ga-rich condition. Most importantly, the treated sample was cooled down in the ultra-high-vacuum chamber to 0 °C (see later) in order to prevent any surface oxidation. Aluminum nanofilm growth started after the residual arsenic vapor in the chamber had been pumped away and the background pressure had been lower than 2×10^{-10} Torr. In our MBE system, the growth rate of the Al films was about 0.366 μm h^{-1}. During the growth of an Al nanofilm, the GaAs substrate holder was not rotating, and no heater power was applied in order to ensure a low growth temperature. We note that in our MBE system the minimum reading of our thermometer is 0 °C. We made sure that the thermometer reading was always 0 °C but in reality, the growth temperature might as well be lower than 0 °C. In any case, the growth temperature was substantially lower than that of the nanofilm presented in our previous work (room temperature) [20].

2.2. Device geometry and stability

The Al sample was processed into a Hall bar geometry. Contact pads made by standard photo lithography are prepared for wire bonding. The key issue is that we use dilute AZ developer in order to avoid etching the Al nanofilm. For an as-grown 4 nm thick Al nanofilm, there are about 17 atomic layers. However, according to our previous work on a similar Al nanofilm [20], there is a $\approx$ 2 nm thick AlO_x layer on top of our Al nanofilm as shown in the TEM studies. When we further consider the surface roughness of our Al 4 nm thick nanofilm (see later), we estimate that there are 7–10 layers of Al atoms. The Al nanofilm devices are stable in air over a long period of time (over 14 months), possibly protected by the overlaying AlO_x layer which is formed when the Al wafer was removed from the MBE chamber for *ex situ* processing.

2.3. Low-temperature four-terminal resistance measurements

The low-temperature transport experiments were performed in an Oxford Triton 200 cryo-free He^3/He^4 dilution refrigerator. The magnetic field is perpendicularly applied to the plane of the Al nanofilm. Although the base temperature of our bottom-loading dilution refrigerator is around 13 mK, the lowest measurement temperature was set at 250 mK. The reason for this is that when the sample undergoes a superconductor/metal transition at a high critical current, huge heat dissipation can occur, and at a temperature below 250 mK the cooling power of our fridge is lower than heat dissipation of our device, leading to an abrupt increase of the measurement temperature.

Standard four-terminal dc resistance measurements were performed on our Al sample. A Keithley 2400 current source was used to provide a constant current which flows between the source and drain contacts. A Keithley 2000 multi-meter

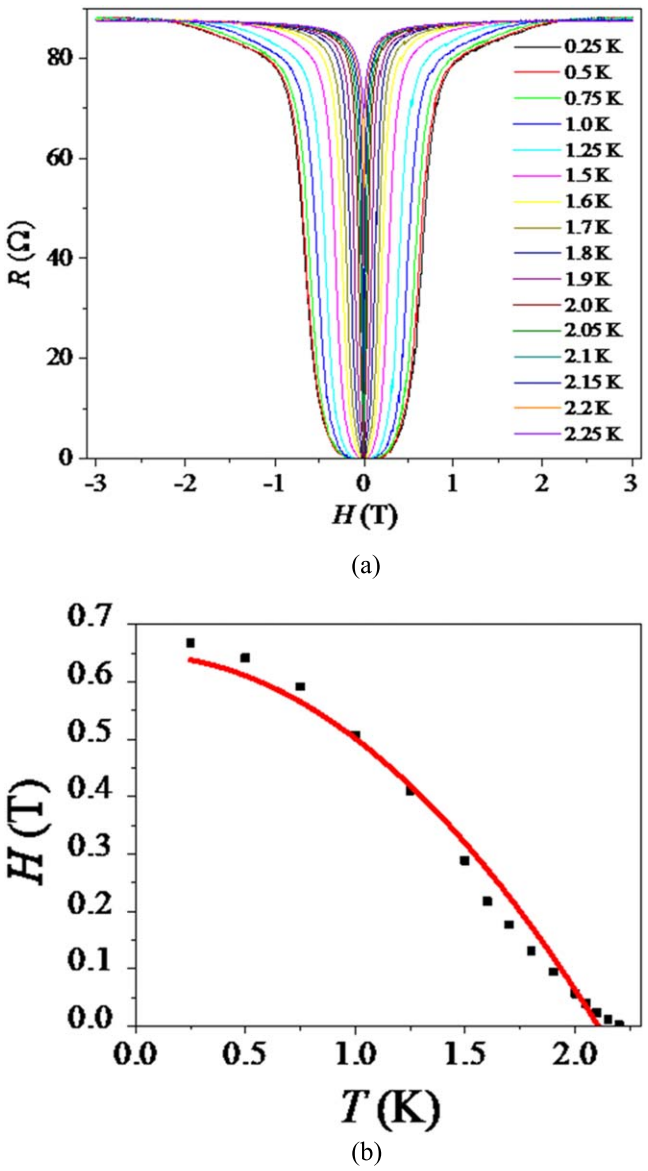

Figure 1. (a) Resistance measurements of the 4 nm thick Al film as a function of magnetic field $R(H)$ for different temperatures T. (b) Upper critical magnetic field as a function of temperature $H_{c2}(T)$. The fit corresponds to the theoretical models.

was used to measure the voltage difference between the voltage probes.

2.4. Superconducting transition temperature and upper critical magnetic field

Figure 1(a) shows magnetoresistance measurements $R(H)$ at various temperatures. The magnetic field is applied perpendicular to the plane of our Al nanofilm. For a certain temperature, the upper critical magnetic field $H_{c2}(T)$ can be measured when the magnetoresistance reaches half of the normal-state resistance value, and such results are shown in figure 1(b). There is a good fit $H_{c2}(T) = H_{C2}(0)[1\text{-}(T/T_c)^2]$ [21, 22] to the data, though there appears to be small deviation from the fit in the high T regime. The critical field $H_{c2}(T = 0)$ and critical temperature T_c are measured to be 0.67 T and 2.21 K, respectively. Both $H_{c2}(T = 0)$ and critical temperature T_c are substantially higher those of bulk Al (0.01 T and 1.2 K). The Ginzburg–Landau coherence length $\xi_{GL} = \sqrt{\frac{h}{4\pi e H_{c2}(T=0)}}$ is measured to be 22 nm.

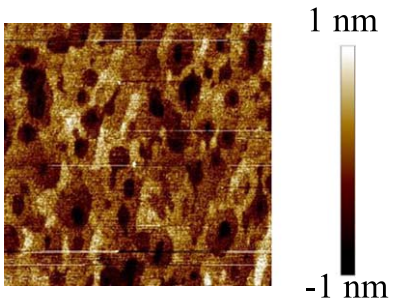

Figure 2. A 5 μm $\times$ 5 μm AFM image of the top surface of the 4 nm thick aluminum film. Note that the scale bar ranges from -1.0 to 1.0 nm.

3. Results and discussion

The 4 nm thick (as grown) Al film reported in this paper was prepared in a Varian Gen-II solid-source MBE system [20]. The quality of the sample in this work is similar to those reported in [20]. According to our previous studies [19, 20], the thinnest continuous Al film which we can prepare is 3 nm thick (as-grown). We decide to study a 4 nm thick Al nanofilm as we wish to further study an Al ultrathin film with a slightly enhanced thickness.

Figure 2 shows a 5 μm $\times$ 5 μm atomic force microscope (AFM) image of the top surface of the 4 nm thick aluminum film. The black regions could correspond to voids in the Al nanofilm which are not conducting and therefore should not affect the transport properties and superconductivity in our Al nanofilm [20]. The root-mean-square (RMS) surface roughness is measured to be 0.4 nm. This value is one order of magnitude lower than that was reported in our previous work [19]. The key issue is that in the present work, the growth temperature (estimated to be much lower 0 °C) is lower than that reported in [19] (room temperature). It may be possible that the low thermal energy provided by the substrate limits the movement of Al atoms when they reach the substrate. In some sense, the Al atoms are stuck onto the GaAs substrate at a low growth temperature, thereby decreasing the RMS surface roughness of Al film. This observation of decreasing RMS surface roughness with decreasing substrate temperature in our Al film is consistent with Al nanofilms on steel grown by RF-magnetron sputtering [23] and Al ultrathin films on glass prepared by electron-beam evaporation [24].

Figure 3 shows the resistance measurements of the Al film as a function of temperature $R(T)$ at zero magnetic field. When the resistance reaches the half value of its normal state, the superconducting transition temperature is measured to be 2.2 K, which is substantially higher than that of bulk Al (1.2 K). Normally the superconducting transition temperature of a thin film is lower than that of a bulk sample. However,

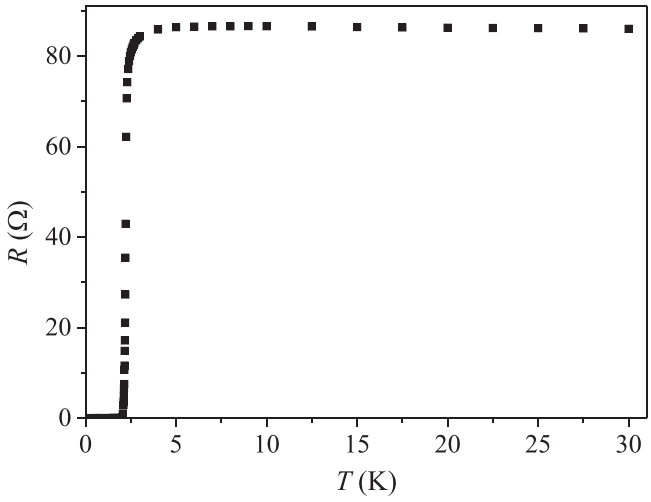

Figure 3. Resistance of the 4 nm thick Al film as a function of temperature $R(T)$ at zero magnetic field.

the opposite trend, that is, an increased T_c measured in thin films compared to those of bulk samples, has been observed in double-atomic-layer Ga films on GaN [25], FeSe monolayer films on $SrTiO_3$ [26] and FeSe on TiO_2 [27]. These interesting results, together with the present work on the MBE-grown Al nanofilm, may indicate that the interface effects play an important role in the enhanced superconductor transition temperature in a nanofilm over that of its bulk counterpart [28]. For example, it has been suggested that the substrate plays an essential role in realizing the high-T_c superconductivity in FeSe (48 K), probably via interface-induced electron–phonon coupling enhancement and charge transfer [27]. On the other hand, a FeTe ultrathin layer grown on a topological insulator substrate does not show superconductivity down to 5 K [28].

In our device, the Ginzburg–Landau coherence length is estimated to be 22 nm, much longer than the as-grown Al film thickness (4 nm). Such results strongly suggest 2D superconductivity in our Al nanofilm. However, one may argue the fact that the Ginzburg–Landau coherence length is much longer than the film thickness may not be sufficient for us to claim 2D superconductivity. To this end, we perform extensive $V(I)$ measurements at different temperatures. The results are shown in figure 4(a). The red lines represent fits $V \sim I^{\alpha}$ to the data at various temperatures. It is possible to obtain two fits over different regions for a fixed temperature. The exponent α tends to decrease with increasing T. Interestingly, in sharp contrast to most experimental results reported in the literature [4, 6–8], there are *two* regions showing behavior consistent with the BKT transition as indicated by the two dashed lines in black (figure 4(a)). As a result, there exist *two* regions in which the *I*–*V* curves show BKT-like characteristics: $T_{BKT} = 1.97$ K in the low voltage region and $T_{BKT} = 2.17$ K in the high voltage region as shown in figure 4(b).

In order to further study the two regions which show BKT-like behavior, we plot $R(T)$ at zero magnetic field for three different source-drain currents, as shown in figure 5. We

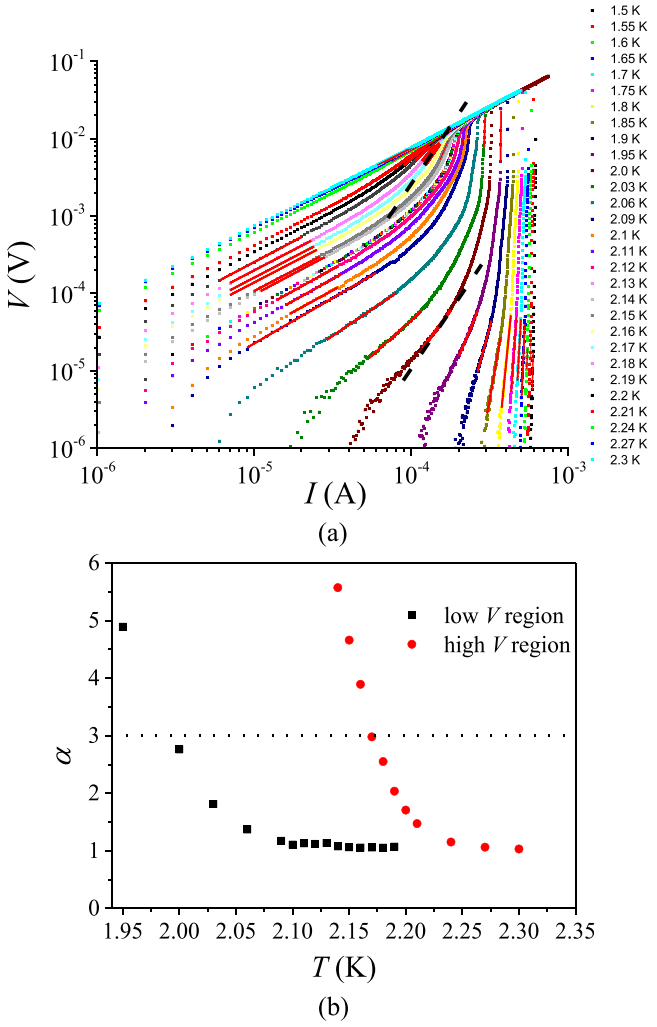

Figure 4. (a) *I*–*V* curves at various temperatures on a log–log scale. The red lines correspond to linear fits $V \sim I^{\alpha}$ to the experimental data. The two black dashed lines corresponds to $V \sim I^3$. (b) The exponent α in the relation $V \sim I^{\alpha}$ obtained from the data shown in figure 4(a).

fit our experimental data to the temperature-induced vortices/antivortices unbinding model [29]

$$R \propto e^{-2\sqrt{\frac{b}{T-T_{BKT}}}}, \quad (1)$$

where b is a constant. We obtain that the parameter T_{BKT} is from 2.16 to 2.2 K, with a slight current dependence which might be a consequence of weak Joule heating as shown in figure 5. However, such a small change of T_{BKT} (0.04 K) observed in this sample over a magnitude of the current show that possible weak Joule heating in the normal state does not prohibit us from determining the correct T_{BKT} using the fits at different currents. The measured T_{BKT} is close to that measured in the high-voltage region in the nonlinear *I*–*V* data.

As the measurement temperature approaches the critical temperature T_c, the fluctuations of a system grow and more time is required before the thermal equilibrium is reached. The characteristic length scale of the fluctuations is described by the correlation length ξ, and the critical behavior of elapsing time τ takes the form: $\tau \propto \xi^z$. Since ξ approaches

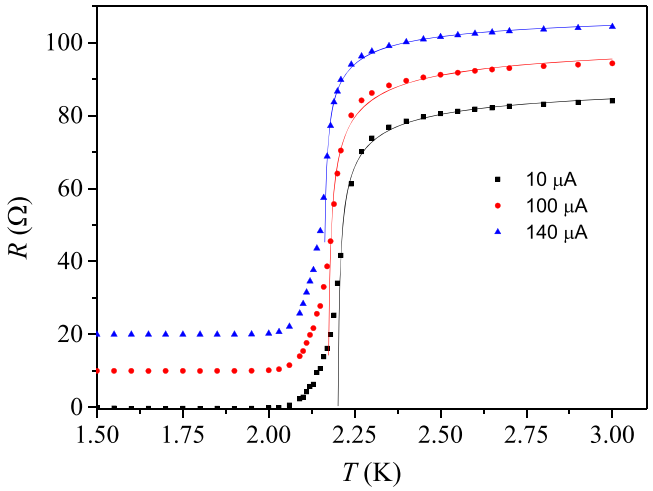

Figure 5. Resistance measurements as a function of temperature at three different source-drain currents. Red (blue) curves have been vertically offset by 10 Ω (20 Ω) for clarity. The continuous curves correspond to a fit to equation (1).

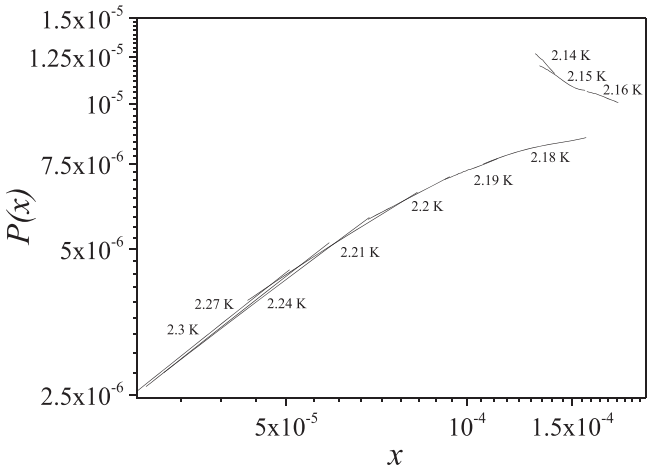

Figure 6. Scaling function (equation (2)) at different temperatures. The upper (lower) branch corresponds to below (above) the critical temperature. The discontinuity yields $T_{\mathrm{BKT}} = 2.17$ K.

infinity as $T \to T_c$, the time taken for thermalization hence diverges. This phenomenon is called critical slowing down and the exponent z is called the dynamical critical exponent. Fisher, Fisher, and Huse [30] derived a theory based on the universal scaling function for a d-dimensional superconductor. According to [30], in our 2D Al nanofilm we have

$$\frac{I}{T}\left(\frac{I}{V}\right)^{\frac{1}{z}} = P_{\pm}\left(\frac{I\xi'}{T}\right), \tag{2}$$

where the symbol $\pm$ denotes above/below T_c, P is the scaling function, $\xi = \xi_0\sqrt{\frac{b}{T-T_{\mathrm{BKT}}}}$, and $\xi' = \sqrt{\frac{b}{T-T_{\mathrm{BKT}}}}$. Given that $\lim_{\xi\to\infty} P_{+}\left(\frac{I\xi'}{T}\right) \to constant$, we obtain $V = (T_{\mathrm{BKT}})^{-z} I^{(1+z)}$ at T_{BKT}. That is equivalent to $V \sim I^3$ with $z = 2$. In our case, the trial value for parameters b, T_{BKT}, and z are declared at first, so $x \equiv \frac{I}{T}e^{-\sqrt{\frac{b}{|T-T_{\mathrm{BKT}}|}}}$ and $P_{\pm}\left(\frac{I\xi}{T}\right) = \frac{I}{T}\left(\frac{I}{V}\right)^{\frac{1}{z}}$ can be calculated by inputting the current and the corresponding voltage at a certain temperature. After that, $P_{\pm}(x)$ can be plotted. Our goal is to find a set of parameters (b, T_{BKT}, z) so that $P_{\pm}(x)$ at different temperatures collapse unto two branches. As shown in figure 6, our analysis gives rise to a critical temperature $T_{\mathrm{BKT}} = 2.17$ K with a dynamical exponent $z = 2$. Again, this value is close to that determined in the $V(I)$ data in the high-voltage region

All the data and analysis shown in figures 5 and 6 as well as the experimental results in the linear transport regime (figure 3) all give rise to a transition temperature of ~2.2 K. These results strongly suggest that the topological transition temperature determined in the high voltage regime as shown in figure 4(b) is the correct $T_{\mathrm{BKT}} \approx 2.17$ K. Our experimental results strongly suggest that the relation $V \sim I^3$ at a certain temperature alone may not be sufficient to accurate determine the transition temperature. The two I–V regions that show BKT-like behavior may have been observed in [5], though the authors did not mention this. It is not clear why I–V curves, which show BKT-like behavior in two regions $V \sim I^3$, are not reported in [4] and [6–8]. Perhaps by lowering the driving current, two regions which show BKT-like behavior could also be observed. We speculate that in our Al nanofilm the BKT-like characteristics in the low voltage region is caused by finite size effects [31]. In this context, near the resistive tail in the low voltage region, free vortices, rather than unbound vortices/antivortices can be created [31].

4. Conclusion

In summary, we have reported extensive transport measurements on a 4 nm thick Al nanofilm on a GaAs substrate grown by MBE. As our Al films can be grown on GaAs, we will be able to integrate Al-based superconductivity, plasmonics, SERS, light-emitting diodes, *etc* with existing GaAs HEMT technology, which could be a great advantage for future device applications. Interestingly, there appear to be *two* regions where the I–V curves are BKT-like. After fitting our experimental data to both the temperature-induced vortices/antivortices unbinding model and the dynamical scaling theory, we conclude that the topological transition temperature $T_{\mathrm{BKT}} = 2.17$ K measured in the high-voltage region is the correct one in our Al superconducting nanofilm. Our work thus demonstrates that in order to unequivocally determine the correct T_{BKT} of superconducting transition, it is imperative to fit one's data to not only the nonlinear I–V model but also the temperature-induced vortices/antivortices unbinding model and the dynamical scaling theory.

Acknowledgments

We thank Professor L-M Wang for useful discussions. We would like to acknowledge the technical support from the Center of Nano Science and Technology and the Center of Nano Facility at National Chiao Tung University. This work was financially supported by the Ministry of Education

(MOE) ATU program, National Taiwan University (NTU) (grant number: 108L892101), and the Ministry of Science and Technology (MOST) (grant number: MOST 105–2112-M-002–005-MY3, MOST 108–2112-M-002–014-MY2, MOST 108-2627-E-002-001, and MOST 108–2622–8–002–016) in Taiwan. The work of AK at NTU was made possible by arrangement with Professor E S Kannan at BITS-Pilani, India. AK was supported by the TEEP@India Program provided by the MOE, Taiwan (grant number: 106M4102–7).

ORCID iDs

Lee Chow https://orcid.org/0000-0001-7729-6848
Chi-Te Liang https://orcid.org/0000-0003-4435-5949

References

[1] Mermin N D and Wagner H 1966 *Phys. Rev. Lett.* **7** 1133–6
[2] Berezinskii V L 1970 *Zh. Eksp. Teor. Fiz.* **59** 907–20
[3] Kosterlitz J M and Thouless D J 1973 *J. Phys. C: Solid State Phys.* **6** 1181–203
[4] Epstein K, Goldman A M and Kadin A M 1981 *Phys. Rev. Lett.* **47** 534–7
[5] Zhao W *et al* 2013 *Solid State Commun.* **165** 59–63
[6] Xing Y *et al* 2015 *Science* **350** 542–5
[7] Wang H *et al* 2017 *Nat. Commun.* **8** 394
[8] Matetskiy A V, Ichinokura S, Bondarenko L V, Tupchaya A Y, Gruznev D V, Zotov A V, Saranin A A, Hobara R, Takayama A and Hasegawa S 2015 *Phys. Rev. Lett.* **115** 147003
[9] Lay C L, Koh C S L, Wang J, Lee Y H, Jiang R, Yang Y, Yang Z, Phang I Y and Lin X Y 2018 *Nanoscale* **10** 575–81
[10] Lee M, Kim J U, Lee K J, Ahn S, Shin Y-B, Shin J and Park C B 2015 *ACS Nano* **9** 6206–13
[11] Zhou L, Tan Y, Wang J, Xu W, Yuan Y, Cai W, Zhu S and Zhu J 2016 *Nat. Photon.* **10** 393–8
[12] Bauch M, Toma K, Toma M, Zhang Q and Dostalek J 2014 *Plasmonics* **9** 781–99
[13] Chou B-T, Chou Y-H, Wu Y-M, Chung Y-C, Hsueh W-J, Lin S-W, Lu T-C, Lin T-R and Lin S-D 2016 *Sci. Rep.* **6** 19887
[14] Cheng C-W, Liao Y-J, Liu C-Y, Wu B-H, Raja S S, Wang C-Y, Li X, Shih C-K, Chen L-J and Gwo S 2018 *ACS Photonics* **5** 2624–8
[15] Lee Y J, Kim H H, Lee Y J, Kim J H, Choi H-J and Choi W K 2019 *Nanotechnology* **30** 035207
[16] Janisch C, Song H, Zhou C, Lin Z, Elías A L, Ji D, Terrones M, Gan Q and Liu Z 2016 *2D Mater.* **3** 025017
[17] Liu J, Yang L, Zhang H, Wang J and Huang Z 2017 *Small* 2017 **13** 1701112
[18] Zai J, Liu Y, Li X, Ma Z-F, Qi R and Qian X 2017 *Nano-Micro Lett.* **9** 21
[19] Lin S-W, Wu Y-H, Chang L, Liang C-T and Lin S-D 2015 *Nanoscale Res. Lett.* **10** 71
[20] Fan Y-T, Lo M-C, Wu C-C, Chen P-Y, Wu J-S, Liang C-T and Lin S-D 2017 *AIP Adv.* **7** 075213
[21] Gorter J C and Casimir H B 1934 *Physika* Z **35** 963
[22] Bardeen J, Cooper L N and Schrieffer J R 1957 *Phys. Rev.* **108** 1175–204
[23] Mwema F M, Oladijo O P and Akinlabi E T 2018 *Mater. Today: Proc.* **5** 20464–73
[24] Her S-C and Wang Y-H 2015 *Indian J. Eng. Mater. Sci.* **22** 268–72
[25] Zhang H-M *et al* 2015 *Phys. Rev. Lett.* **114** 107003
[26] Ge J-F, Liu Z-L, Liu C, Gao C-L, Qian D, Xue Q-K, Liu Y and Jia J-F 2015 *Nat. Mater.* **14** 285–9
[27] Ding H, Lv Y-F, Zhao K, Wang W-L, Wang L, Song C-L, Chen X, Ma X-C and Xue Q-K 2016 *Phys. Rev. Lett.* **117** 067001
[28] Eich A *et al* 2016 *Phys. Rev.* B **94** 125437
[29] Halperin B I and Nelson D R 1979 *J. Low Temp. Phys.* **36** 599–617
[30] Fisher D S, Fisher M P A and Huse D A 1981 *Phys. Rev.* B **43** 130–59
[31] Holzer J, Newrock R S, Lobb C J, Aouaroun T and Herbert S T 2001 *Phys. Rev.* B **63** 184508